Colloids and Surfaces A: Physicochem. Eng. Aspects 462 (2014) 45–51

Contents lists available at ScienceDirect

Colloids and Surfaces A: Physicochemical and Engineering Aspects

journal homepage: www.elsevier.com/locate/colsurfa

Evaluation of modified silica nanoparticles in carboxylated nitrile rubber nanocomposites

Renata L. Sala[a], Tatiane M. Arantes[a], Elson Longo[a], Edson R. Leite[a], Caio M. Paranhos[b], Emerson R. Camargo[a,*]

[a] LIEC – Interdisciplinary Laboratory of Electrochemistry and Ceramics, Department of Chemistry, UFSCar-Federal University of São Carlos, Rod. Washington Luis km 235, CP 676, 13565-9905 São Carlos, SP, Brazil

[b] Department of Chemistry, UFSCar – Federal University of São Carlos, Rod. Washington Luis km 235, CP 676, São Carlos, SP 13565-9905, Brazil

HIGHLIGHTS

- We modified silica nanoparticles with a silane agent and with a polymeric shell.
- SiO_2 nanoparticles induced arrangements in XNBR nanocomposites.
- The SDS induced the polymeric macromolecules organization in the nanocomposites.
- The silica nanoparticles dispersed in the polymer forming a mass fractal system.
- The silica nanoparticles and XNBR chains formed three-dimensional network.

GRAPHICAL ABSTRACT

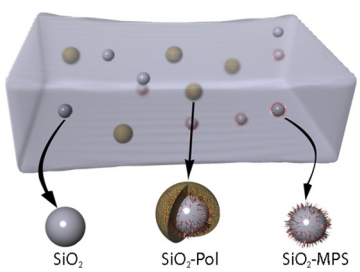

ARTICLE INFO

Article history:
Received 11 May 2014
Received in revised form 23 July 2014
Accepted 19 August 2014
Available online 27 August 2014

Keywords:
Silica nanoparticles
Modified surface
Polymer nanocomposites
Colloidal route

ABSTRACT

Surface-modified silica nanoparticles have a plenty of applications, such as coatings, dyes or biomarkers, catalysts and encapsulated products. When modified with 3-(trimethoxysilyl)propyl methacrylate (SiO_2-MPS) or covered with a polymeric shell obtained from a reaction between divinylbenzene and styrene (SiO_2-Pol), these SiO_2 nanoparticles induced distinct arrangements in polymer nanocomposites (PNC) prepared with commercial carboxylated nitrile rubber (XNBR). The hydrophilicity character of the modified SiO_2 nanoparticles was also altered, improving their interaction with the XNBR macromolecules. Consequently, choosing the PNC properties for different conditions and applications became possible due to the adjustment of the nanoparticle surface characteristics. Although the final characteristics of the nanocomposites films varied according to the nanoparticle used, the PNC prepared with SiO_2-Pol presented better homogeneity than those with SiO_2-MPS.

1. Introduction

Numerous efforts have been focused on the search for new materials involving lower cost, greater durability and, especially, lower environmental impact. In this sense, polymer nanocomposites (PNC) become the focus of many research groups owing to their superior mechanical and thermal properties. The field of PNC is of growing interest due to the remarkable properties that result from the effect of nanofillers in the polymer on macro and micro scales

* Corresponding author at: LIEC-Department of Chemistry, UFSCar-Federal Universisty of São Carlos, Rod. Washington Luis km 235, CP 676, São Carlos, SP 13565-905, Brazil. Tel.: +55 16 3351 8090; fax: +55 16 3351 8350.

E-mail addresses: renata.lang89@gmail.com (R.L. Sala), tmarantes@yahoo.com.br (T.M. Arantes), elson@iq.unesp.br (E. Longo), edson.leite@pq.cnpq.br (E.R. Leite), paranhos@ufscar.br (C.M. Paranhos), camargo@ufscar.br (E.R. Camargo).

http://dx.doi.org/10.1016/j.colsurfa.2014.08.012
0927-7757/

[1–8]. It has been shown that a system of well-dispersed nanoparticles usually improve composite properties, since agglomerates of particles can generate voids that act as preferential sites for failure, reducing its general performance [9].

Silica nanoparticles with different morphologies, such as spherical [2,10], core/shell [11,12], network [13] and mesoporous [14], have been studied for many applications such as adhesives, industrial coatings, electronic matrices and encapsulated pesticides and drugs [11,15,16]. As fillers in PNC, spherical SiO_2 can improve the interaction between the polymer and the inorganic phase [15]. However, their agglomeration, due to the dominant Van der Waals interactions, has been an obstacle to its wide application [9].

Silica nanoparticles with the surface modified were found to steadily disperse nano-SiO_2 in many organic media [12,17,18]. Furthermore, the silica-core/organic-shell also improves the interaction at the organic/inorganic interface and has been applied in different technological fields [17]. The synthesis of silica/polymer hybrid particles usually is reached via physical or physicochemical interaction between silica particles and the polymer or directly through the polymerization on the surface of nanoparticles. In the meantime, the morphology of hybrid particles that results from the shell polymerization are hard to control and significantly low encapsulation efficiency has been observed [11,12]. Von Werne et al. [19] obtained well-defined polymer-nanoparticle hybrids modifying the surface of silica nanoparticles with initiators for atom transfer radical polymerization (ATRP). They used these initiator-modified nanoparticles as macro initiators, but only small nanoparticles exhibited good control of the polymer molecular weight. On the other hand, McDonald et al. [20] reported a different approach to prepare hollow polymeric microspheres by a process that initially involved the polymerization of chains with low molecular weight, such as styrene, containing a small amount of carboxylic acid [12,20–22].

The purpose of this study was to improve the dispersion of three different kind of silica nanoparticles (unmodified SiO_2, silica with its surface modified with silane groups and silica covered with a polymeric shell obtained from a polymerization reaction) in a matrix of carboxylated nitrile rubber (XNBR), as well as to understand the organic/inorganic interface between the polymer and the nanoparticles with modified hydrophobic and hydrophilic characteristics. Furthermore, we investigated how nanocomposites structures changed when different interfacial groups were used between the nanoparticles and the polymeric matrix.

2. Experimental

2.1. Synthesis

Silica nanoparticles were synthesized through the hydrolysis and controlled condensation of tetraethyl orthosilicate (TEOS 98%, Aldrich, USA). A solution of 25 mL of distilled water, 35 mL of absolute ethanol, and 0.51 mol of NH_3 from an aqueous solution (30%, analytical grade, Synth, Brazil) was prepared and immediately added to a second solution prepared with 35 mL of ethanol and 26.4 mmol of TEOS under vigorous stirring, resulting in a colloidal dispersion of SiO_2 nanoparticles. After 4 h, the surface of the SiO_2 particles was modified by adding 200 μL of 3-(trimethoxysilyl)propyl methacrylate (MPS) coupling agent (98%, Aldrich, USA) directly into the silica dispersion, which was maintained under continuous stirring for 24 h at room temperature. The functionalized SiO_2-MPS nanoparticles were purified by repeated centrifugation and washed with ethanol to separate the nanoparticles by their size, as well as to remove any excess of NH_3 and MPS.

To cover the silica surface with the polymer shell, 50 mL of SiO_2-MPS nanoparticles were dispersed in ethanol (4 mg mL^{-1}) and mixed with 2 mL of a solution prepared with 120 mg of polyvinylpyrrolidone (Aldrich, EUA) and 2 mL of anhydrous ethanol, followed by the addition of 3 mL from a solution prepared with 1980 μL of styrene (>99%, Aldrich, EUA), 2463 μL of divinylbenzene (DVB) (80%, Aldrich, EUA), 360 mg of azobisisobutyronitrile (AIBN) (DuPont, Brazil) and 3 mL of anhydrous ethanol. The reaction was heated to 60 °C using a silicone oil bath under constant stirring for 5 h. After polymerization, the coated nanospheres (SiO_2-Pol) were separated from the suspension by centrifugation and washed with ethanol. The monomers were firstly washed with an aqueous solution of NaOH (5%, Synth, Brazil), distilled water and dried with $MgSO_4$ (PA, Vetec, Brazil) to remove the inhibitor prior to use.

The PNC films were prepared by a colloidal synthesis route mixing commercial polymer lattices of XNBR (43.7% of solids and 25% of acrylonitrile, Nitriflex, Brazil) with the colloidal dispersions of silica nanoparticles. Aqueous colloidal dispersions of pure SiO_2, SiO_2-MPS and SiO_2-Pol nanoparticles (5% in mass) were prepared in the presence of 0.1 mol L^{-1} of sodium dodecyl sulfate (SDS) to improve the nanoparticle dispersion. After that, they were added to the XNBR lattice, gently homogenized for 1 h, dried in Petri dishes in an air circulation oven at 50 °C and then deployed as self-sustained PNC films. One film of XNBR with only SDS was prepared to understand the surfactant influence in the inorganic/organic interface.

2.2. Characterization

The morphology, size, and size distribution of SiO_2, SiO_2-MPS and SiO_2-Pol nanoparticles were analyzed by FTIR, HRTEM and SEM. The infrared spectra were collected at room temperature in the range of 400–4000 cm^{-1} with 32 scans and 4 cm^{-1} of resolution in a FTIR infrared spectrometer (Bruker Equinox 55) with a diffuse reflectance accessory. Diluted nanoparticle dispersions of SiO_2-Pol were dripped on copper grids covered with a thin amorphous carbon film to collect images in a TECNAI F20 field emission HRTEM operating at 200 kV. Scanning electron microscopy images of the SiO_2-MPS nanoparticles were recorded with a JEOL JSM-5600LV operated at 20 kV. Transmittance infrared spectra of nanocomposites films and of pure MPS were collected at room temperature in the range from 650 to 4000 cm^{-1} with 32 scans and 4 cm^{-1} of resolution in a FTIR infrared spectrometer (Bruker Equinox 55) with an attenuated total reflectance accessory (ZnSe monocrystal). DSC curves were taken with a Netzsch Phoenix 204 calorimeter in the range from −100 to +100 °C at a heating rate of 20 °C min^{-1}. X-ray diffraction (XRD) patterns were recorded at room temperature using a LabX XRD-6000 Shimadzu diffractometer operating with Cu K_α radiation, in the 2θ range of 3–30°, in step scan mode with a width of 0.02° and a step time of 2 s. Experiments of SAXS, which provided valuable information about their structural features at a nanometer-level, providing statistical and overall information averaged in a volume in the order of 1 mm^3, were performed in a Bruker AXS 2D Nanostar (EUA) with CuK_α radiation, operating at 40 kV/35 mA in a range of 0.01–0.23 Å^{-1}. The sample-to-detector distance was fixed at 107 cm, and the time-resolved spectra of nanocomposites were collected every 1200 s, with a minimum resolution in q = 0.00628 Å^{-1}.

3. Results and discussion

Monodispersed SiO_2 nanoparticles were prepared by the method originally proposed by Stöber et al. [23] and recently optimized by Arantes et al. [24]. To improve and understand the inorganic/organic interface between the nanoparticle and the

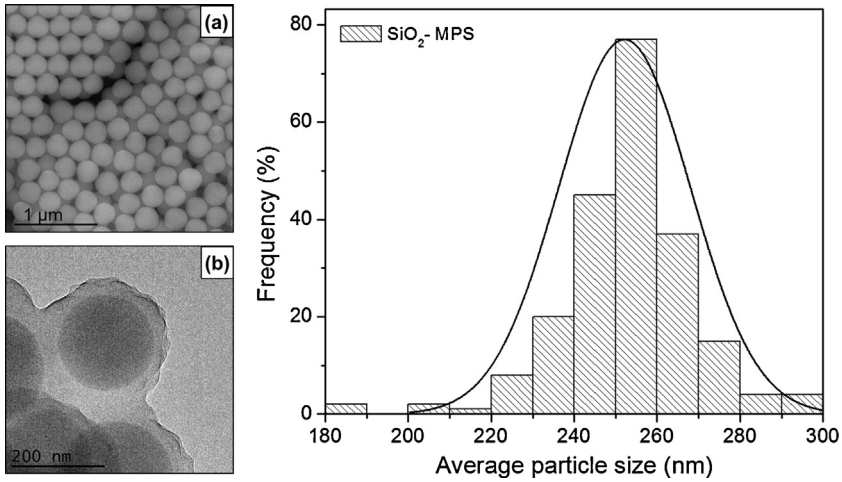

Fig. 1. (a) SEM image of SiO_2-MPS and its histogram; (b) HRTEM image of SiO_2-MPS covered with the polymer shell.

polymer aiming to obtain better PNC, the SiO_2 surface was modified reacting the silanol groups of the nanoparticles with hydrolyzed MPS. This reaction takes approximately 24 h in an EtOH/H_2O mixture at room temperature, and it is expected to form siloxanes in competition with the MPS oligomerization reaction [10]. The presence of the MPS coupling agent attaches polymerizable vinyl groups on the SiO_2, which results in monodispersed core/shell functional hybrid nanospheres by the copolymerization of styrene and DVB. The reactive vinyl groups were used here as seeds for the growth of the polymer shell layer, with the DVB acting as

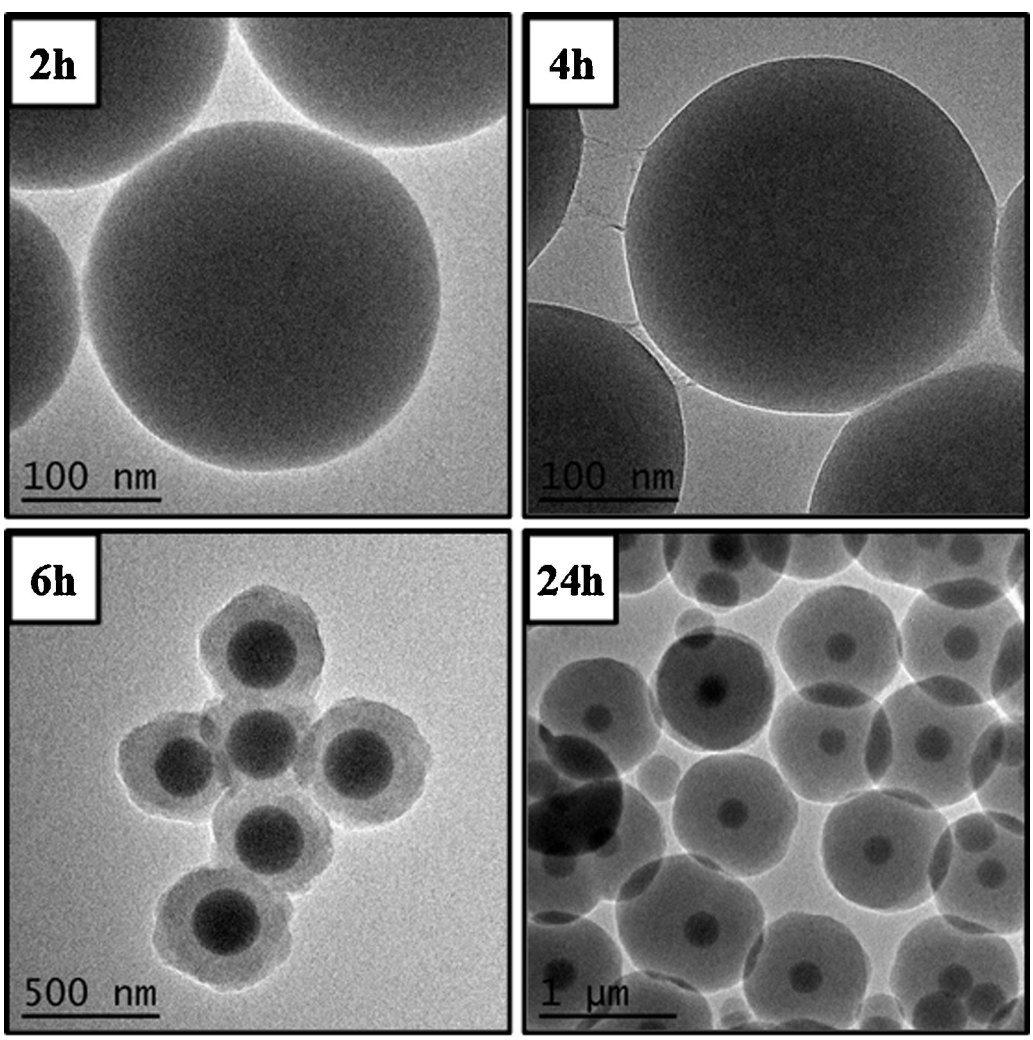

Fig. 2. HRTEM images of SiO_2-MPS covered with the polymer shell after 2,4,6 and 24 h of reaction time.

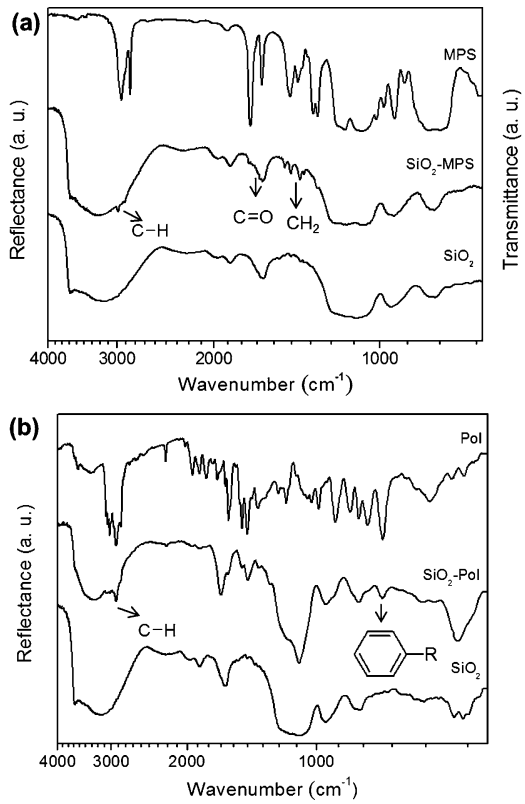

Fig. 3. (a) Reflectance FTIR spectra of SiO_2, SiO_2-MPS and transmittance FTIR spectrum of pure MPS; (b) reflectance FTIR spectra of SiO_2, SiO_2-Pol and pure styrene and DVB polymerized.

crosslinker and AIBN as radical initiator [12,22]. The SEM image of Fig. 1a shows spherical SiO_2-MPS nanoparticles with a smooth surface and a narrow size distribution. The histogram of Fig. 1 revels an average diameter of 250 nm and a standard deviation of 23 nm, in good agreement with a recent optimized model based on a multivariate approach [24]. On the other hand, the HRTEM image of Fig. 1b shows the silica nanoparticles covered with a polymer shell (SiO_2-Pol) with a thickness greater than 20 nm after 5 h of reaction, which indicates that the technique is quite efficient to obtain the polymer shell around silica nanoparticles.

Fig. 2 shows the polymeric shell thickness increasing with the reaction progress after 2, 4, 6 and 24 h, indicating that the shell thickness could be controlled by the monomer concentration, polymerization time and molecular weight of the polymer molecules. Particularly, the control of the thickness of core/shell nanoparticles broadens the PNC applicability, which can be used as dyes and inks, protector of light-sensitive compounds, in heterogeneous catalysts and to prepare encapsulated compounds [21,25–27].

The functionalization of silica with MPS groups is highlighted in the SiO_2-MPS FTIR spectrum (Fig. 3) by the presence of the peak at 1713 cm^{-1} due to the C=O stretching and by peaks in the range of 1190–1140 cm^{-1} corresponding to the C—C(=O)— stretch of esters, which overlap the strong absorption at 1106 cm^{-1} of the Si—O—Si symmetrical vibration [28]. The presence of MPS onto the silica surface is evidenced by the peaks in the 1450–1323 cm^{-1} region corresponding to in plane and out of plane bending CH_2 vibrations [28], also presented in the SiO_2-Pol spectrum from the polymeric shell formed by styrene and DVB. A peak of C=C from the silane group at 1635 cm^{-1} is partially overlapped by the band of untreated asymmetrical vibration of the silica centered at 800 cm^{-1} [10,12,29]. According to Bauer et al. [30], the complete disappearance of the MPS band at 2847 cm^{-1} in the SiO_2-MPS spectrum is due the splitting of methoxy groups during the grafting

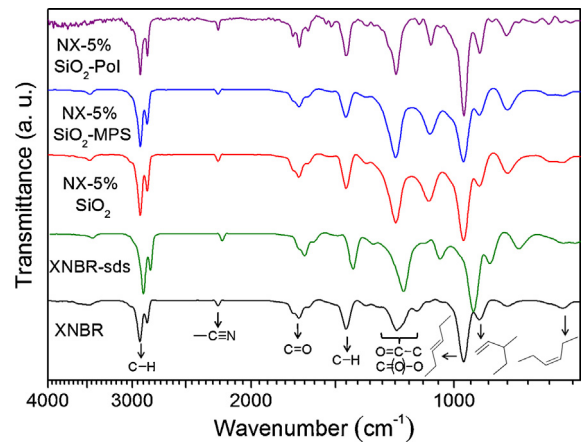

Fig. 4. Infrared spectra of XNBR, XNBR in the presence of SDS surfactant and XNBR nanocomposites (NX) with 5% of SiO_2, 5% of SiO_2-MPS and 5% of SiO_2-Pol.

process. Furthermore, the absence of the silanol band at 3670 cm^{-1} confirms the covalent bonds between the methoxy functional groups and the silanol groups of the SiO_2 surface [30].

In the case of SiO_2-Pol, its spectrum shows the presence of the typical phenyl absorption of the styrene and DVB at 705 cm^{-1} and the asymmetrical stretching of CH_2 at 2916 cm^{-1} overlapped by the OH stretching vibrations of Si-OH [12], which was also observed in the SiO_2-MPS spectrum at 2979 cm^{-1} [28].

When silica nanoparticles (SiO_2-MPS or SiO_2-Pol) were inserted in the XNBR to form PNC, their FTIR spectra show differences compared to the spectrum of pure XNBR, especially in the range 800–1400 cm^{-1} (Fig. 4). This region consists of two asymmetrical coupled vibrations at 1192 and 1130 cm^{-1} from the carboxylate anion, out-of-plane bending in 1350–1150 cm^{-1} and the sulfate stretching of the SDS surfactant in 1415–1380 cm^{-1} and 1200–1185 cm^{-1}. The vibrational modes associated to the butadiene bands appear at 964 cm^{-1} (trans 1,4-butadiene), 915 cm^{-1} (1,2 butadiene) and at 694 cm^{-1} (cis 1,4-butadiene) [28,29]. These results suggest that the carbonyl groups and the double bonds of butadiene groups are interacting with silica nanoparticles. Nanocomposites with 1% and 5% of SiO_2-MPS show some bands shifted to higher wavenumber, indicating that the energetic condition of the polymer chains was modified due the presence of nanoparticles.

The microscopic structure of the samples was studied by XRD, which is normally used to identify long-range order of crystalline materials. In this study, both silica and the polymeric matrix present an amorphous halo in their XRD patterns (Fig. 5). Nevertheless, the nanocomposites showed some diffraction intensities between 3–10° and 20–25°. These peaks were also observed in the XRD pattern of the dry surfactant powder and their presence in the patterns of PNC can be related to SDS arrangements formed during the film drying [31]. The shift of these peaks to smaller angles in the XRD pattern of the PNC indicates a larger intermolecular spacing between the SDS molecules in the presence of the XNBR rubber. Since the surfactant was initially dissolved in water aiming to facilitate the dispersion of nanoparticles into the polymer and the homogeneity of the PNC, it seems that the intermolecular arrangements of the SDS were promoted by the functional groups of the polymer, especially the carboxylates.

The SDS and similar surfactants have been extensively applied in emulsion polymerization [32,33], synthesis of core/shell particles [34] and to improve the dispersion of single and multi-wall carbon nanotubes (SWNT and MWNT) [35–37] or silica [38–40] in different polymeric matrices. Its use can promote a preferential adsorption of the sulfate polar group on the surface of the nanoparticles by

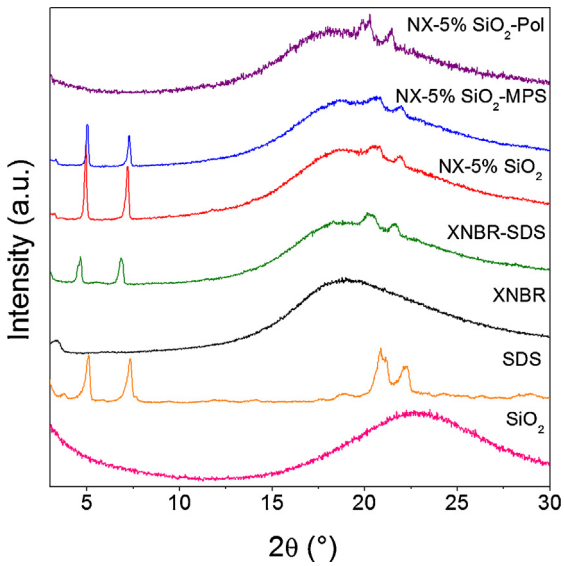

Fig. 5. XRD patterns for XNBR, XNBR in the presence of SDS surfactant and nanocomposites with 5% of SiO_2, 5% of SiO_2-MPS and 5% of SiO_2-Pol.

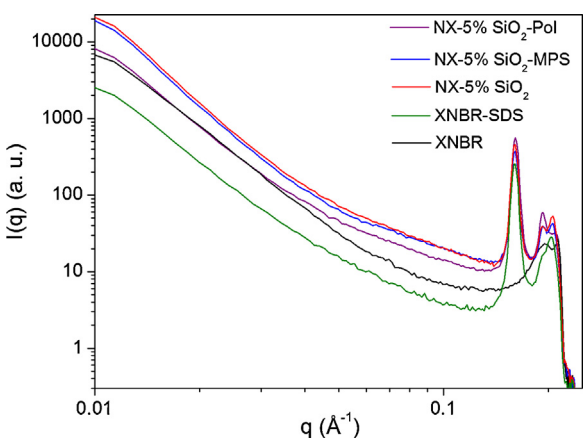

Fig. 6. SAXS intensity, $I(q)$, as a function of the scattering vector, q, for XNBR, XNBR in the presence of SDS surfactant and nanocomposites with 5% of SiO_2, 5% of SiO_2-MPS and 5% of SiO_2-Pol.

electrostatic interaction, reducing the formation of agglomerates in organic media [38]. However, the behavior of SDS in the PNC films has not been fully investigated yet. Among the PNC with different modified SiO_2, the sample with 5% SiO_2-Pol seems to have the best nanoparticle distribution and homogeneity, since only two small broad peaks were observed in the XRD patterns. The polymer shell might have reduced the silica hydrophilic character and aggregation in the final nanocomposite [38], interacting their phenyl groups with the XNBR matrix.

The morphology of the nanocomposites was also investigated by SAXS, which provided additional information about the average distance between possible domains present in the samples and the correlation volume associated to their spatial distribution, the organic–inorganic phase boundary and its degree of ramification [27]. This technique is adequate to study the structure of hybrid materials because of the contrast in electronic densities between organic–inorganic phases at nanoscale, and provides valuable information about their structural features from the statistical information averaged in a volume of approximately 1 mm^3 [32].

Fig. 6 shows the SAXS intensity as a function of the scattering vector (q) of different PNC and XNBR. In the profile of pure polymer, small broad peaks at $q = 0.2\,Å^{-1}$ appear probably due to intramolecular and intermolecular nanodomains spatially correlated that originated from interactions of the XNBR functional groups. These peaks are also present in all the PNC scattering curves, but with different intensities. The average distance between these domains (d) embedded in the continuous polymeric matrix were calculated by the Bragg equation (Eq. (1)) and are shown in Table 1 [27,41,42].

$$d = \frac{2\pi}{q_{max}} \tag{1}$$

The correlation volume associated to the spatial distribution of the nanodomains (L_c) shown in Table 1 were estimated by the Scherrer equation for SAXS (Eq. (2)), where Δq is the full-width at half-maximum of the correlation peaks [41,43].

$$L_c = \frac{4\pi}{\Delta q} \tag{2}$$

All the d and L_c values were calculated from SAXS curve, showing three small broad bands at $q = 0.163$, 0.196 and 0.207 $Å^{-1}$. For these bands, the correlation volume associated to the spatial distribution of nanodomains increased for the nanocomposites and for the polymer with SDS, possibly due to the increase of the matrix density in the presence of nanoparticles [43] and the formation of small polymeric nanodomains distributed for all the material. This result can be related to a better dispersion of nanoparticles, favoring regions where the nanodomains are spatially correlated. When larger segregation is present, the low dispersion degree can result in a three-dimensional network of nanoparticles, restraining the extension of regions where silica and XNBR nanodomains are spatially correlated [43]. Furthermore, the presence of silica nanoparticles could have formed coacervates of XNBR, leading to a new arrangement of XNBR domains with different sizes.

On the other hand, the materials synthesized with the surfactant showed an intensity scattering at $q = 0.160\,Å^{-1}$, probably related to an intramicellar form factor resulted from the electronic density of the polar SDS shell formed in the XNBR polymer domain [44]. Romani et al. [44] studied sodium dodecyl sulfate micelles systems in different conditions of pH interacting with drugs, solvents and at distinct shapes such as prolate ellipsoid, cylinder and esferic, by SAXS [44–48]. They reported that the SDS monomers may reassemble into cylinder-like aggregates to accommodate the polar headgroups from poly(ethylene glycol) and poly(N-vinyl-2-pyrrolidone), mediating their interaction in this ternary system of surfactant and water-soluble polymers [44].

$$I(q) \propto q^{-D} \tag{3}$$

More information about the aggregation state could be obtained from the Porod equation (Eq. (3)) described for the middle q region (0.01–0.1 $Å^{-1}$) and obtained from the log-log SAXS curves in the Fig. 7 [27,43]. In this equation, D is the power law exponent that is correlated with the fractal dimension, quantifying the manner in which the mass of an object increases with length. This exponent reflects an averaging over the power law distribution of cluster sizes and provides information about the surface roughness of the hierarchical structures formed in the nanocomposites [27,43,49–51]. Schaefer et al. [49,51] distinguished the morphology of various sol–gel derived materials based on silica, describing $1 < D < 3$ for polymeric precursors, $3 < D < 4$ for rough colloids, $D = 4$ for smooth colloids and $D > 4$ for surfactant-coated colloidal particles. In this study, the exponent D found for the PNC was between 2 and 3 (Table 1), indicating a mass fractal of polymeric structure with open three-dimensional network of weakly branched polymeric system [49,52]. In general, the larger the fractal dimension, the more connected is the structure [37]. In this sense, smaller D values obtained for the nanocomposites when compared to the pure copolymer indicate that the silica nanoparticles, especially the SiO_2 covered

Table 1
d,L_c, D, T_g values calculated for XNBR and nanocomposites.

Samples	q = 0.163 Å^{-1}		q = 0.196 Å^{-1}		q = 0.207 Å^{-1}		D (Å)	T_g (°C)
	d (Å)	L_c (Å)	d (Å)	L_c (Å)	d (Å)	L_c (Å)		
XNBR	38	215	32	457	29	1802	3.03	−19.8
XNBR-sds	39	477	33	923	31	942	2.74	−22.7
NX-5% SiO_2	39	403	33	1023	31	1096	2.84	−22.9
NX-5% SiO_2-MPS	39	457	32	704	30	1119	2.73	−18.9
NX-5% SiO_2-Pol	39	421	33	1104	30	908	2.61	−19.6

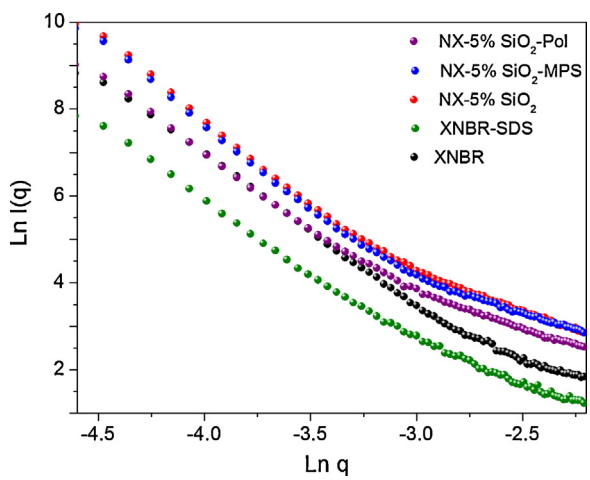

Fig. 7. Ln-Ln SAXS curves for the middle q region (0.01–0.1 Å^{-1}) of pure XNBR, XNBR in the presence of SDS surfactant and nanocomposites with 5% of SiO_2, 5% of SiO_2-MPS and 5% of SiO_2-Pol.

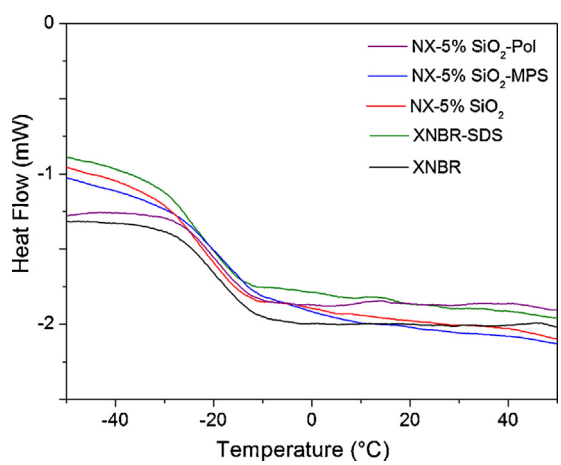

Fig. 8. DSC curves for pure XNBR, XNBR in the presence of SDS surfactant and nanocomposites with 5% of SiO_2, 5% of SiO_2-MPS and 5% of SiO_2-Pol.

with the polymer shell and the surfactant reduced the dense polymeric chains interconnection in the final materials.

Glass transition temperatures (T_g) of the PNC were determined from the DSC analysis and the values are listed in Table 1. Fig. 8 shows the DSC curves of the nanocomposites prepared with different nanoparticles, where can be noted that the XNBR-SDS and NX-5% SiO_2 samples have lower T_g than the pure polymer due to the higher mobility of the polymer chains surrounding the nanoparticles and a possible increase in the spacing and free volume by the presence of nanoparticles, which restricts the extent of regions where nanodomains of silica, surfactant and XNBR are spatially correlated [53]. Mélé et al. [53] also reported that data from SAXS and atomic force microscopy confirmed that higher silica content leads to greater three-dimensional percolation of its network formed in the polymer matrix, resulting in a superior mobility of the nanocomposites.

For the NX-5% SiO_2-MPS and NX-5% SiO_2-Pol nanocomposites, the T_g values were slightly higher than in the pure polymer, i.e., the presence of nanoparticles may have reduced the mobility of the polymer chains, probably due to a better interaction between the organic/inorganic phases [15]. Liu and Zhao [12] also observed an increased of 2 °C in the T_g of styrene-butadiene rubber (SBR) nanocomposites with the insertion of nanosilica by colloidal route, followed by the coagulation of the latex. According to the authors, the rise in T_g was due to the restricted mobility of the SBR chains resulted from the strong interfacial interaction of the silica nanoparticles with the polymeric matrix.

Additionally, changes in heat capacity at T_g (ΔC_p) may reveal some relaxation aspects of the amorphous rigid content in XNBR matrix. As can be seen in Fig. 8, the presence of SiO_2, SiO_2-Pol or SiO_2-MPS fillers did not cause significant changes in ΔC_p. This behavior indicates that the interaction between modified silica nanoparticles and XNBR was not sufficiently intense to promote a rigid interfacial phase, which is consistent with the coacervated state observed by SAXS.

4. Conclusions

Polymer nanocomposites films were prepared by a colloidal synthesis route mixing commercial polymer lattices of XNBR and surface modified silica nanoparticles with 3-(trimethoxysilyl)propyl methacrylate (SiO_2-MPS) or covered with a polymeric shell obtained from a reaction between divinylbenzene and styrene (SiO_2-Pol). When introduced into the XNBR matrix, these nanoparticles were dispersed in the polymeric nanodomain arrangements, forming a mass fractal system and coacervated structures with open three-dimensional network of linked nanoparticles and XNBR chains. The shell thickness of SiO_2-Pol nanoparticles was successfully controlled varying the polymerization time and seems to have improved their dispersion in the polymeric media and enhanced the interface between the inorganic/organic phases. Additionally, the SDS surfactant induced the organization of the polymeric macromolecules in the nanocomposites, retaining its intramicellar form factor and crystalline structure in the final nanocomposite films. The use of different modifying agents on the silica surface generated distinct polymeric domains and dispersion in a polymeric matrix, controlling the final nanocomposite structure.

Acknowledgments

Authors acknowledge the Brazilian agencies São Paulo Research Foundation (FAPESP) (grants 2012/07067-0 and 2012-05013-0), CNPq and CAPES for financial support, the INCTMN/CMDMC, and Nitriflex by the XNBR commercial lattices.

References

[1] F.R. Costa, S. Pradhan, U. Wagenknecht, A.K. Bhowmick, G. Heinrich, XNBR/LDH nanocomposites: effect of vulcanization and organic modifier on nanofiller

dispersion and strain-induced crystallization, J. Polym. Sci. B: Polym. Phys. 48 (2010) 2302–2311.
[2] M.J. Percy, J.I. Amalvy, D.P. Randall, S.P. Armes, S.J. Greaves, J.F. Watts, Synthesis of vinyl polymer-silica colloidal nanocomposites prepared using commercial alcoholic silica sols, Langmuir 20 (2004) 2184–2190.
[3] J.W.J. Gilman, C.L. Jackson, A.B. Morgan, R.J. Harris, Flammability properties of polymer-layered-silicate nanocomposites. Polypropylene and polystyrene nanocomposites, Chem. Mater. 12 (2000) 1866–1873.
[4] J.M. Zhu, A.B. Morgan, F.J. Lamelas, C.A. Wilkie, Fire properties of polystyrene-clay nanocomposites, Chem. Mater. 13 (2001) 3374–3780.
[5] E. Manias, A. Touny, L. Wu, K. Strawhecker, B. Lu, T.C. Chung, Polypropylene/montmorillonite nanocomposites. Review of the synthetic routes and materials properties, Chem. Mater. 13 (2001) 3516–3523.
[6] T.M. Kashiwagi, A.B. Morgan, J.M. Antonucci, M.R. VanLandingham, R.H. Harris, W.H. Awad, J.R. Shields, Thermal and flammability properties of a silica-poly(methylmethacrylate) nanocomposite, J. Appl. Polym. Sci. 89 (2003) 2072–2078.
[7] T.M. Arantes, K.V. Leão, M.I.B. Tavares, A.G. Ferreira, E. Longo, E.R. Camargo, NMR study of styrene-butadiene rubber (SBR) and TiO_2 nanocomposites, Polym. Test. 28 (2009) 490–494.
[8] J. Oberdisse, Aggregation of colloidal nanoparticles in polymer matrices, Soft Matter 2 (2006) 29.
[9] V.S. Gowri, L. Almeida, T. Amorim, N. Carneiro, A.P. Souto, M.F. Esteves, Novel copolymer for SiO_2 nanoparticles dispersion, J. Appl. Polym. Sci. 124 (2012) 1553–1561.
[10] S. Borsacchi, M. Geppi, C.A. Veracini, F. Fallani, L. Ricci, G. Ruggeri, Improving compatibility in LDPE-silica dispersions by photo-grafting reaction. Preparation and solid state NMR investigation, J. Mater. Chem. 16 (2006) 4581.
[11] E. Bourgeat-Lami, J. Lang, Encapsulation of inorganic particles by dispersion polymerization in polar media: 1. Silica nanoparticles encapsulated by polystyrene, J. Colloid Interface Sci. 197 (1998) 293–308.
[12] G. Liu, L. Li, X. Yang, Z. Dai, Preparation of silica/polymer hybrid microspheres and the corresponding hollow polymer microspheres with functional groups, Polym. Adv. Technol. 19 (2008) 1922–1930.
[13] L. Matějka, O. Dukh, J. Kolařík, Reinforcement of crosslinked rubbery epoxies by in-situ formed silica, Polymer 41 (2000) 1449–1459.
[14] H. Yang, Y. Liu, Q. Shen, L. Chen, W. You, X. Wang, J. Sheng, Mesoporous silica microcapsule-supported Ag nanoparticles fabricated via nano-assembly and its antibacterial properties, J. Mater. Chem. 22 (2012) 24132.
[15] Y.-C. Chiu, H.-C. Tsai, T. Imae, Thermal and morphology properties of various silica contents in sulfone epoxy nanocomposites, J. Appl. Polym. Sci. 125 (2012) E523–E531.
[16] K.G. Das, Controlled-Release Technology: Bioengineering Aspects, Wiley, New York, 1983.
[17] X. Li, Z.-J. Zhan, G.-R. Peng, W.-K. Wang, Comprehensive high-performance epoxy nanocomposites co-reinforced by organo-montmorillonite and nano-SiO_2, J. Appl. Polym. Sci. 123 (2012) 3503–3510.
[18] D.K. Yi, S.S. Lee, G.C. Papaefthymiou, J.Y. Ying, Nanoparticle architectures templated by SiO_2/Fe_2O_3 nanocomposites, Chem. Mater. 18 (2006) 614–619.
[19] T. von Werne, T.E. Patten, Atom transfer radical polymerization from nanoparticles: a tool for the preparation of well-defined hybrid nanostructures and for understanding the chemistry of controlled/living radical polymerizations from surfaces, J. Am. Chem. Soc. 123 (2001) 7497–7505.
[20] C.J. McDonald, K.J. Bouck, A.B. Chaput, C.J. Stevens, Emulsion polymerization of voided particles by encapsulation of a nonsolvent, Macromolecules 33 (2000) 1593–1605.
[21] T.K. Mandal, M.S. Fleming, D.R. Walt, Production of hollow polymeric microspheres by surface-confined living radical polymerization on silica templates, Chem. Mater. 12 (2000) 3481–3487.
[22] X. Xu, S.A. Asher, Synthesis and utilization of monodisperse hollow polymeric particles in photonic crystals, J. Am. Chem. Soc. 126 (2004) 7940–7945.
[23] W. Stöber, A. Fink, E. Bohn, Controlled growth of monodisperse silica spheres in the micron size range, J. Colloid Interface Sci. 26 (1968) 62–69.
[24] T.M. Arantes, A.H. Pinto, E.R. Leite, E. Longo, E.R. Camargo, Synthesis and optimization of colloidal silica nanoparticles and their functionalization with methacrylic acid, Colloid Surf. A 415 (2012) 209–217.
[25] K. Kamata, Y. Lu, Y. Xia, Synthesis and characterization of monodispersed core–shell spherical colloids with movable cores, J. Am. Chem. Soc. 125 (2003) 2384–2385.
[26] M. Okubo, Y. Konishi, H. Minami, Production of hollow polymer particles by suspension polymerization, Colloid. Polym. Sci. 276 (1998) 638–642.
[27] S. Yano, K. Kurita, K. Iwata, T. Furukawa, M. Kodomari, Structure and properties of poly(vinyl alcohol)/tungsten trioxide hybrids, Polymer 44 (2003) 3515–3522.
[28] R.M. Silverstein, F.X. Webster, D. Kiemle, The Spectrometric Identification of Organic Compounds, 7th ed., John Wiley & Sons, New York, 2005.
[29] T.M. Arantes, R.L. Sala, E.R. Leite, E. Longo, E.R. Camargo, Comparison of the nanoparticles performance in the photocatalytic degradation of a styrene–butadiene rubber nanocomposite, J. Appl. Polym. Sci. 128 (2013) 2368–2374.
[30] F. Bauer, H. Ernst, U. Decker, M. Findeisen, H.-J. Gläsel, H. Langguth, E. Hartmann, R. Mehnert, C. Peuker, Preparation of scratch and abrasion resistant polymeric nanocomposites by monomer grafting onto nanoparticles, 1 FTIR and multi-nuclear NMR spectroscopy to the characterization of methacryl grafting, Macromol. Chem. Phys. 201 (2000) 2654–2659.
[31] L.A. Smith, R.B. Hammond, K.J. Roberts, D. Machin, G. McLeod, Determination of the crystal structure of anhydrous sodium dodecyl sulphate using a combination of synchrotron radiation powder diffraction and molecular modelling techniques, J. Mol. Struct. 554 (2000) 173–182.
[32] K. Landfester, N. Bechthold, F. Tiarks, M. Antonietti, Miniemulsion polymerization with cationic and nonionic surfactants: a very efficient use of surfactants for heterophase polymerization, Macromolecules 32 (1999) 2679–2683.
[33] F. Tiarks, K. Landfester, M. Antonietti, Silica nanoparticles as surfactants and fillers for latexes made by miniemulsion polymerization, Langmuir 17 (2001) 5775–5780.
[34] Y. Guo, M. Wang, H. Zhang, G. Liu, L. Zhang, X. Qu, The surface modification of nanosilica, preparation of nanosilica/acrylic core–shell composite latex, and its application in toughening PVC matrix, J. Appl. Polym. Sci. 107 (2008) 2671–2680.
[35] K.P.T. Nair, P. Thomas, R. Joseph, Latex stage blending of multiwalled carbon nanotube in carboxylated acrylonitrile butadiene rubber: mechanical and electrical properties, Mater. Des. 41 (2012) 23–30.
[36] O. Regev, P.N.B. ElKati, J. Loos, C.E. Koning, Preparation of conductive nanotube–polymer composites using latex technology, Adv. Mater. 16 (2004) 248–251.
[37] L.H. Sperling, Introduction to Physical Polymer Science, 4th ed., John Wiley & Sons, Hoboken, 2005.
[38] H. Zou, S. Wu, J. Shen, Polymer/silica nanocomposites: preparation, characterization, properties, and applications, Chem. Rev. 108 (2008) 3893–3957.
[39] T.-M. Wu, M.-S. Chu, Preparation and characterization of thermoplastic vulcanizate/silica nanocomposites, J. Appl. Polym. Sci. 98 (2005) 2058–2063.
[40] Y.H. Lai, M.C. Kuo, J.C. Huang, M. Chen, On the PEEK composites reinforced by surface-modified nano-silica, Mater. Sci. Eng. A 458 (2007) 158–169.
[41] H.S. Mansur, R.L. Oréfice, A.A.P. Mansur, Characterization of poly(vinyl alcohol)/poly(ethylene glycol) hydrogels and PVA-derived hybrids by small-angle X-ray scattering and FTIR spectroscopy, Polymer 45 (2004) 7193–7202.
[42] K. Dahmouche, C.V. Santilli, M. Da Silva, C.A. Ribeiro, S.H. Pulcinelli, A.F. Craievich, Silica–PEG hybrid ormolytes: structure and properties, J. Non-Cryst. Solids 247 (1999) 108–113.
[43] C.M. Paranhos, K. Dahmouche, S. Zaioncz, B.G. Soares, L.A. Pessan, Relationships between nanostructure and thermomechanical properties in poly(vinyl alcohol)/montmorillonite nanocomposite with an entrapped polyelectrolyte, J. Polym. Sci. B: Polym. Phys. 46 (2008) 2618–2629.
[44] A.P. Romani, M.H. Gehlen, R. Itri, Surfactant–polymer aggregates formed by sodium dodecyl sulfate, poly(N-vinyl-2-pyrrolidone), and poly(ethylene glycol), Langmuir 21 (2004) 127–133.
[45] R. Itri, L.Q. Amaral, Small-angle X-ray scattering of systems with inhomogeneous particles, J. Appl. Crystallogr. 27 (1994) 20–24.
[46] C.V. Teixeira, R. Itri, L.Q. do Amaral, Micellar shape transformation induced by decanol: a study by small-angle X-ray scattering (SAXS), Langmuir 16 (2000) 6102–6109.
[47] W. Caetano, E.L. Gelamo, M. Tabak, R. Itri, Chlorpromazine and sodium dodecyl sulfate mixed micelles investigated by small angle X-ray scattering, J. Colloid Interface Sci. 248 (2002) 149–157.
[48] M.G. D'Andrea, C.C. Domingues, S.V. Malheiros, F.G. Neto, L.R. Barbosa, R. Itri, F.C. Almeida, E. de Paula, M.L. Bianconi, Thermodynamic and structural characterization of zwitterionic micelles of the membrane protein solubilizing amidosulfobetaine surfactants ASB-14 and ASB-16, Langmuir 27 (2011) 8248–8256.
[49] D.W. Schaefer, Polymers, fractals, and ceramic materials, Science 243 (1989) 1023–1027.
[50] S. Disch, The spin structure of magnetic nanoparticles and in magnetic nanostructures, 2011.
[51] D. Schaefer, K. Keefer, Fractal geometry of silica condensation polymers, Phys. Rev. Lett. 53 (1984) 1383–1386.
[52] S. Neves, C. Polo Fonseca, Determination of fractal dimension of polyaniline composites by SAXS and electrochemical techniques, Electrochem. Commun. 3 (2001) 36–43.
[53] P. Mélé, S. Marceau, D. Brown, Y. de Puydt, N.D. Albérola, Reinforcement effects in fractal-structure-filled rubber, Polymer 43 (2002) 5577–5586.